THE JOURNAL OF PHYSICAL CHEMISTRY A
A JOURNAL OF THE AMERICAN CHEMICAL SOCIETY

pubs.acs.org/JPCA Article

# Excited-State Intramolecular Proton Transfer in Salicylidene-α-Hydroxy Carboxylate Derivatives: Direct Detection of the Triplet Excited State of the *cis*-Keto Tautomer

Geethika K. Weragoda, Nayera M. Abdelaziz, Dmitrii Govorov,[⊥] Rajkumar Merugu,[⊥] Leanna J. Patton,[⊥] Jennifer E. Grabo,[⊥] R. A. A. Upul Ranaweera, Anna C. Ratliff, W. Dinindu Mendis, Noha Ahmed, Katrin H. Vilinsky, Manabu Abe, Michael J. Baldwin, and Anna D. Gudmundsdottir*

Cite This: *J. Phys. Chem. A* 2023, 127, 2765−2778 Read Online

ACCESS | Metrics & More | Article Recommendations | Supporting Information

**ABSTRACT:** Excited-state intramolecular hydrogen transfer on the triplet surface of salicylideneaniline derivatives has received much less attention than the corresponding ultrafast process on the singlet surface. To enhance the understanding of this triplet reactivity, the photochemical properties of a series of salicylidene-α-hydroxy acid salts with different substituents on the phenol moiety (**1**−**3**) were characterized. UV/vis absorption and phosphorescence measurements in ethanol revealed that **1**−**3** exist as both enol and keto tautomers, with the enol form being predominant. Irradiation of **1** at 310 nm in ethanol glass (77 K) yielded an absorption band with a $\lambda_{max}$ at ∼405 nm, which was assigned to the *trans*-keto tautomer (*trans*-**1K**). In contrast, laser flash photolysis of **1**−**3** in methanol or acetonitrile resulted in a transient absorption with $\lambda_{max}$ at 440−460 nm. This transient, which decayed on the microsecond timescale and was significantly shorter lived in methanol than in acetonitrile, was assigned to the triplet excited state ($T_1$) of the *cis*-keto tautomer (*cis*-**1K**−**3K**) and residual absorption of *trans*-**1K**−**3K** by comparison with TD-DFT calculations. The assignment of the $T_1$ of *cis*-**1K** was further supported by quenching studies with anthracene and 2,5-dimethyl-2,4-hexadiene. Laser flash photolysis of **1** in the temperature range of 173−293 K gave an activation barrier of 6.7 kcal/mol for the decay of the $T_1$ of *cis*-**1K**. In contrast, the calculated activation barrier for *cis*-**1K** to undergo a 1,5-H atom shift to reform **1** was smaller, indicating that intersystem crossing of the $T_1$ of *cis*-**1K** is the rate-determining step in the regeneration of **1**.

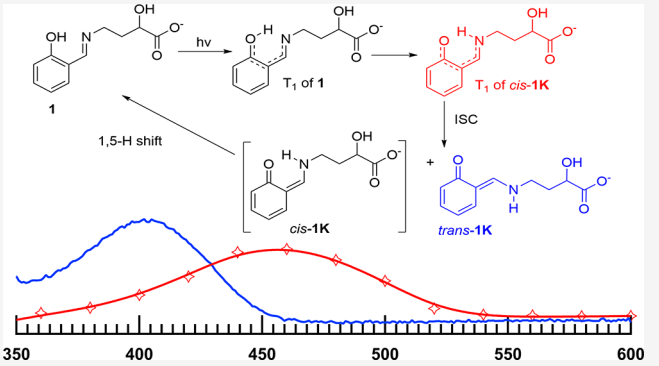


## 1. INTRODUCTION

Hydrogen transfer reactions are of fundamental interest because of their general importance in chemical and biological processes. Light can be used to initiate proton transfer in the excited states of molecules.[1] For example, salicylideneaniline derivatives, which are Schiff bases with an *ortho*-phenolic moiety adjacent to an imino nitrogen atom, undergo excited-state intramolecular hydrogen transfer (ESIPT). Upon excitation, the phenol proton is transferred intramolecularly to the imino nitrogen atom, giving the singlet excited state of the *cis*-keto tautomer, which can undergo bond rotation to form the *trans*-keto tautomer. The excited keto tautomers decay to their ground states by either radiative or nonradiative processes, where the proton is again transferred to reform the enol tautomer (Scheme 1). The *cis*-keto tautomer reforms the enol via an intramolecular 1,5-H atom shift, whereas reformation of the enol from the *trans*-keto tautomer involves a solvent-mediated process.

ESIPT in salicylideneaniline derivatives has been widely investigated.[1−4] Because ESIPT on the singlet surfaces of salicylideneaniline derivatives is a nearly barrierless process, it occurs on an ultrafast timescale. The efficiency and rate of ESIPT make these molecules useful in applications such as optical data storage, molecular processors, fluorescence cell imaging, and chemical sensing.[2,5−8] The photophysical and photochemical properties of salicylideneaniline derivatives that undergo ESIPT have been characterized extensively using various spectroscopic methods, such as femtosecond laser flash photolysis and fluorescence, but these studies have mainly focused on ESIPT in singlet excited states. In contrast, only a few studies have examined ESIPT in the triplet excited states of salicylideneaniline derivatives, and it is generally not known

Received: January 24, 2023
Revised: February 28, 2023
Published: March 16, 2023

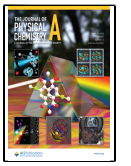







https://doi.org/10.1021/acs.jpca.3c00543
J. Phys. Chem. A 2023, 127, 2765−2778

**Scheme 1. Typical ESIPT in Salicylideneaniline Derivatives**

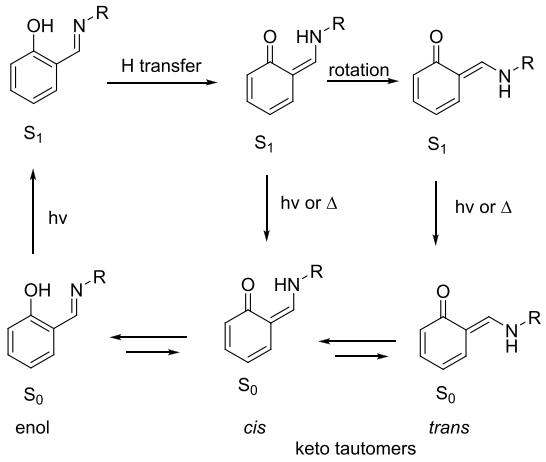


**Scheme 2. Structure of the Schiff Bases 1, 2, and 3 Studied in this Paper, Shown with and without Intramolecular Hydrogen Bonding (Conformers A and B) and Corresponding Keto Tautomers (*cis*- and *trans*-K)**

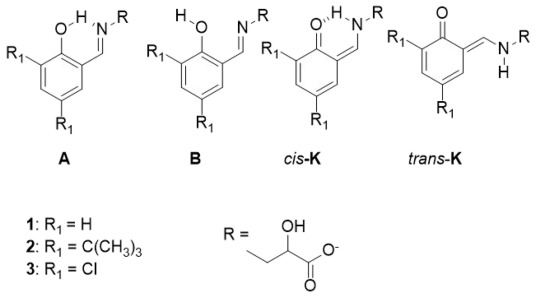


which derivatives intersystem cross to their triplet surface or how efficient their rate of intersystem crossing is.[9−24] Although ESIPT on triplet surfaces occurs on a much slower timescale than that on singlet surfaces, this process has potential utility for applications such as triplet sensitization and triplet−triplet annihilation reactions.[24]

In this article, we report the photochemical properties of a series of salicylidene-$\alpha$-hydroxy acid salts (**1**−**3**; Scheme 2), in which only the presence of electron-donating or electron-withdrawing groups on the phenol moiety was varied. Using nanosecond laser flash photolysis, absorption spectroscopy, phosphorescence, and theoretical calculations, we demonstrated that upon exposure to light, these molecules undergo efficient enol−keto tautomerization through H transfer on the triplet surface to yield the triplet excited state ($T_1$) of the keto tautomer (**K**), which has a lifetime of several microsecond in solution and intersystem crosses to form mainly the *cis*-keto tautomer (*cis*-**K**). However, the *cis*-**K** tautomer was not detectable because it decays faster than its triplet precursor through a 1,5-H atom shift to regenerate **1**−**3**.

## 2. METHODS

**2.1. Molecular Modeling.** All geometries were optimized at the B3LYP, M06-2X, or MP2 level of theory with the 6-31 + G(d) basis set, as implemented in Gaussian16.[25−28] Transition states were confirmed to have one imaginary vibrational frequency by analytical determination of the second derivative of the energy with respect to the internal coordinates. Intrinsic reaction coordinate (IRC) calculations were used to verify that the located transition states corresponded to the attributed reactant and product.[29,30] TD-DFT calculations[31,32] were also performed at the B3LYP level of theory with the 6-31 + G(d) basis set to locate the excited singlet and triplet states of the ground state minimal energy conformer.[33] We used CPCM solvation to model the absorption of the excited state and intermediates.[34,35]

DLPNO-CCSD(T)[36] and DFT calculations were carried out in ORCA 4.2.1[37,38] with the RIJCOSX approximation for integrations over Gaussian-type orbitals (described in ORCA documents). The integration grids used were finer than the ORCA 4.2.1 default: "Grid4 FinalGrid5" for RIJK and "Grid4 FinalGrid5 GridX5" for RIJCOSX. CPCM has been described elsewhere.[39,40]

**2.2. Laser Flash Photolysis.** Laser flash photolysis was performed using an excimer laser (308 nm, 17 ns) or a Nd:YAG laser (266 nm, 3 ns). The systems have been described in detail elsewhere.[41,42] In a typical experiment, a stock solution of **1**−**3** was prepared in spectroscopic grade methanol or acetonitrile, such that the absorption at 308 or 266 nm was between 0.3 and 0.6. Typically, ∼1 mL of the stock solution was placed in a 10 mm × 10 mm, 48 mm long quartz cuvette and then purged with argon or oxygen for 5 min. The rates were obtained by fitting an average of two to three kinetic traces.

**2.3. Preparation of 1−3.** Compounds **1**−**3** were prepared using a previously described procedure.[43] The compounds were characterized by IR, $^1$H-, and $^{13}$C-NMR spectroscopy. The NMR spectra of **1**−**3** fit with those in the literature.[43]

*2.3.1. Sodium Salt of 2-Hydroxy-4-[[(2-hydroxyphenyl)-methylene]amino]butanoic Acid **1**.* $^1$H NMR (400 MHz, $CD_3OD$): $\delta$ 1.80 (m, 1H), 2.10 (m, 1H), 3.70 (t, 2H), 3.95 (t, 1H), 6.72 (m, 2H), 7.22 (m, 2H), 8.45 (s, 1H) ppm. $^{13}$C NMR (101 MHz, $CD_3OD$): $\delta$ 35.7, 53.8, 69.6, 117.1, 117.3, 118.1, 131.5, 132.6, 164.0, 165.7, 179.4 ppm. IR (neat): 3220, 1637, 1590 cm$^{-1}$.

*2.3.2. Sodium Salt of 4-[[[3,5-Bis(1,1-dimethylethyl)-2-hydroxyphenyl]methylene]amino]-2-hydroxy-butanoic Acid **2**.* $^1$H NMR (400 MHz, $CD_3OD$): $\delta$ 1.26 (s, 9H), 1.40 (s, 9H), 1.91 (m, 1H), 2.14 (m, 1H), 3.71 (t, 2H), 4.02 (t, 1H), 7.13 (s, 1H), 7.31 (s, 1H), 8.42 (s, 1H) ppm. $^{13}$C NMR (101 MHz, $CD_3OD$): $\delta$ 28.4, 30.4, 33. 5, 34.4, 36.1, 55.3, 69.7, 118.0, 125.7, 126.0, 135.8, 139.5, 157.9, 166.5, 179.7 ppm. IR (neat): 3250, 2952, 1588, 1529 cm$^{-1}$.

*2.3.3. Sodium Salt of 4-[[(3,5-Dichloro-2-hydroxyphenyl)-methylene]amino]-2-hydroxy-butanoic Acid **3**.* $^1$H NMR (400 MHz, $CD_3OD$): $\delta$ 2.05 (m, 1H), 2.17 (m, 1H), 3.82 (t, 2H), 4.05 (t, 1H), 7.26 (s, 1H), 7.40 (s, 1H), 8.43 (s, 1H) ppm. $^{13}$C NMR (101 MHz, $CD_3OD$): $\delta$ 34.5, 50.0, 69.6, 116.2, 117.4, 125.8, 130.2, 133.7, 165.6, 178.6 ppm. IR (neat): 3256, 2923, 1642, 1601 cm$^{-1}$.

## 3. RESULTS

**3.1. UV/Vis Absorption Spectra of 1−3.** We used absorption spectroscopy to determine whether the enol or keto tautomers of **1**−**3** (Scheme 2) are predominant in acetonitrile and ethanol. In dry acetonitrile, **1** and **2** did not show significant absorption above 370 nm (Figure 1A), indicating that they exist mainly in their enol forms as the keto tautomers are expected to be absorbed at longer wavelengths due to their higher conjugation.[5] In contrast, **3** in acetonitrile exhibited significant absorption below 260 nm and above 350 nm ($\lambda_{max}$ = 425 nm), indicating that both the enol and keto tautomers are present. However, in ethanol, absorption


https://doi.org/10.1021/acs.jpca.3c00543
J. Phys. Chem. A 2023, 127, 2765−2778

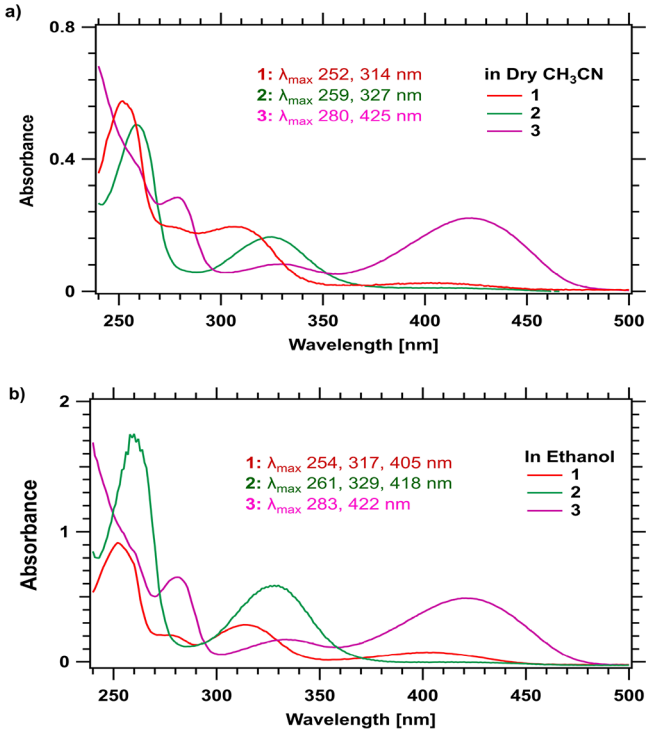


**Figure 1.** Absorption spectra of **1**−**3** (0.2 mM) in (a) dry acetonitrile and (b) ethanol.

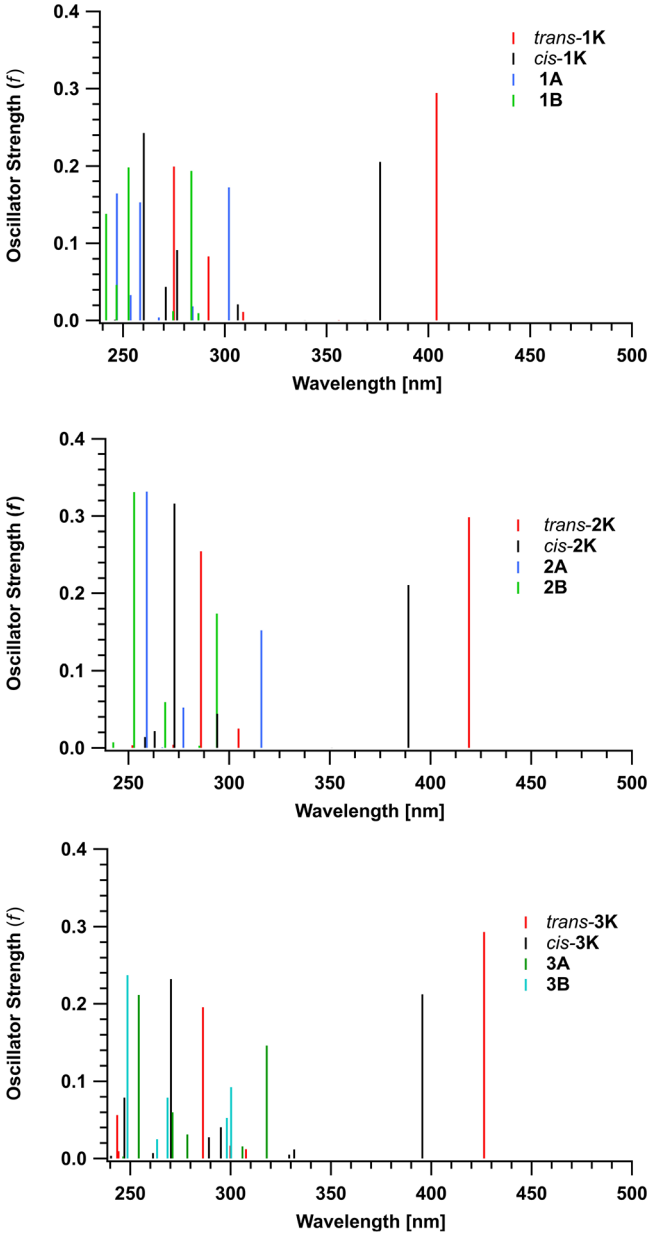


**Figure 2.** TD-DFT-calculated absorption spectra for enols **1A**−**3A** and **1B**−**3B** and their keto tautomers *trans*- and *cis*-**1K**−**3K** using CPCM for solvation in ethanol.

bands above 400 nm were observed for **1** (Figure 1B), suggesting that its keto tautomers is further stabilized in ethanol, whereas **2** and **3** have similar absorption in ethanol and acetonitrile.

To confirm that the absorption at longer wavelengths is due to the keto tautomers, we compared the electronic transitions calculated for *cis*- and *trans*-**1K**−**3K** and those calculated for **1**−**3** with and without intramolecular hydrogen bonding (conformers A and B, respectively; Figure 2). The electronic transitions were calculated using time-dependent density functional theory (TD-DFT) at the B3LYP level of theory with the 6-31 + G(d) basis set[26,44] and the conductor-like polarizable continuum model (CPCM)[34,35] for solvation in both acetonitrile and ethanol. According to the calculations, the enol forms of **1**−**3** do not absorb significantly above 320 nm, whereas the *cis*- and *trans*-keto tautomers have significant absorption above 370 nm.

**3.2. Low-Temperature UV/Vis Absorbance Studies of 1.** To verify that **1** is photochromic and forms its keto tautomer **1K** upon irradiation, it was irradiated in ethanol glass at 77 K. The absorption spectrum of **1** has a major absorption band at ∼310 nm and a smaller one at 405 nm due to **1K** (Figure 1B). Irradiation of **1** with a 310 nm monochromatic light obtained from a Xenon lamp (500 W) resulted in gradual growth of the absorption band at 405 nm as the irradiation time increased (Figure 3). We assigned this absorption band to *trans*-**1K** (Scheme 3) because the TD-DFT-calculated electron transition for *trans*-**1K** at 404 nm ($f$ = 0.294) corresponds well with the observed spectra, whereas the major electronic transition for *cis*-**1K** is located at a shorter wavelength of 376 nm ($f$ = 0.206) (Figure 2). It should be noted that initially the absorbance maximum is centered at ∼420 nm, but upon irradiation, it increasingly shifts to 405 nm. Therefore, we theorize that upon exposure to light, *trans*-**1K** absorbs to twist or rotate to yield rotamers with slightly different absorption until a photoequilibrium is reached. Presumably, the flexible side arm of *trans*-**1K** is involved in forming more stable rotameters, especially those involving solvation of the NH and $CO_2$ moieties.

**3.3. Phosphorescence.** To characterize the $T_1$ of **1**−**3** and the triplet precursors to the keto tautomers ($T_1$ of **1K**−**3K**), we obtained the phosphorescence spectra of **1**−**3** in ethanol matrices at 77 K (Figure 4). These compounds all display dual phosphorescence, with an intense component at shorter wavelengths and a significantly weaker component at longer wavelengths. The phosphorescence at shorter wavelengths has resolved vibrational features, as typically observed for triplet excited states with (n,$\pi^*$) configurations.[45] This emission was assigned to the $T_1$ of **1**−**3** because the energies for the (0,0) bands fit well with the TD-DFT calculated energies (Table 1).



https://doi.org/10.1021/acs.jpca.3c00543
J. Phys. Chem. A 2023, 127, 2765−2778

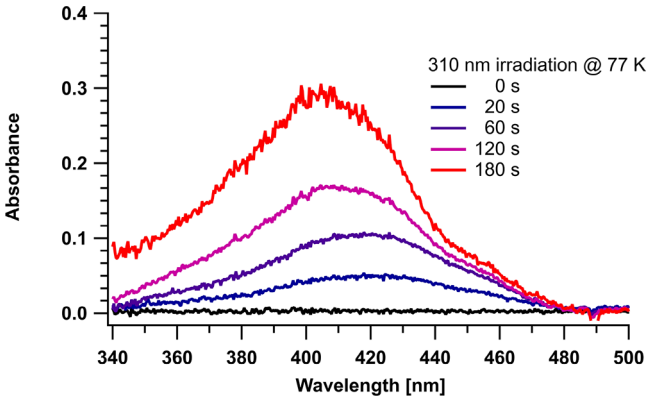


**Figure 3.** Absorption spectra of **1** in ethanol (0.1 mM) at 77 K as a function of irradiation time at 310 nm. Irradiation of **1** with a 310 nm monochromatic light obtained from a Xenon lamp (500 W) resulted in gradual growth of the absorption band at 405 nm as the irradiation time increased.

**Scheme 3. Formation of Keto Tautomers (*cis*- and *trans*-1K) upon Irradiation of Conformers A and B of 1 at 310 nm**

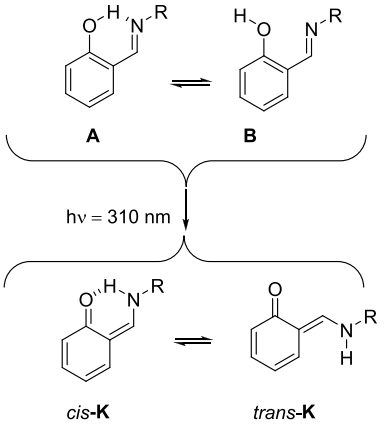


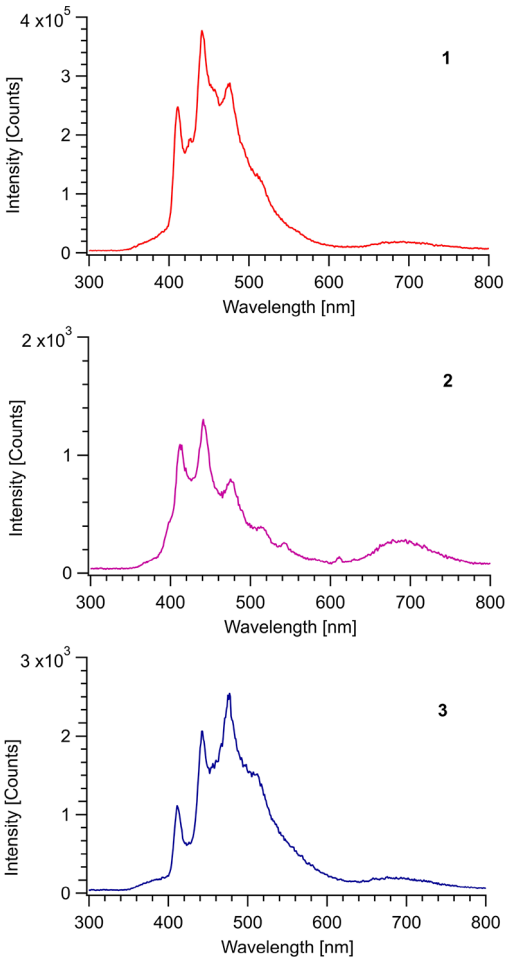


**Figure 4.** Phosphorescence spectra of **1**−**3** in ethanol at 77 K. Phosphorescence was obtained by irradiating **1** with 277 nm light and **2** and **3** with 260 nm light.

We assigned the featureless phosphorescence at longer wavelengths to the $T_1$ of **1K**−**3K**. Because the emission is weak, it is difficult to estimate its onset accurately. Moreover, the TD-DFT-calculated energies for the $T_1$ of *cis*- and *trans*-**1K**−**3K** show that the *cis*-isomer is generally only a few kcal/mol higher in energy than the *trans*-isomer (Table 1). Therefore, we could not determine accurately whether the emission originates from the *trans*- and/or *cis*-isomer, although the calculated energies fit better with *trans*-**1K**−**3K**. Nevertheless, the phosphorescence and absorption spectra of **1**−**3** demonstrate that both the enol and keto tautomers are present in ethanol glass.

**3.4. Laser Flash Photolysis.** Because **1**−**3** and keto tautomers **1K**−**3K** show phosphorescence, we investigated whether the corresponding $T_1$ could be detected using laser flash photolysis and attempted to verify that the $T_1$ of **1**−**3** is the precursor of the $T_1$ of **1K**−**3K**. Laser flash photolysis (308 nm) of **1** in argon- and oxygen-saturated acetonitrile resulted in transient spectra with a major absorption peak at ∼460 nm and a shoulder at ∼300 nm (Figure 5A). Similar transient spectra with a $\lambda_{max}$ at 460 nm were obtained in hexamethylphosphoramide (HMPA), whereas in argon- and oxygen-saturated methanol, the $\lambda_{max}$ was shifted slightly to ∼440 nm.

The transient absorption was assigned by comparison with the TD-DFT-calculated spectra of **1K**, the $T_1$ of **1**, and the $T_1$ of **1K** (Figure 5B). In the TD-DFT-calculated spectrum (acetonitrile, CPCM) of *cis*-**1K**, the major electron transition is located at 372 nm ($f$ = 0.2153). Furthermore, as mentioned previously, the absorption band with a $\lambda_{max}$ at 405 nm obtained by irradiating **1** in ethanol at 77 K corresponded well to the calculated spectrum of *trans*-**1K**. As these calculated spectra do not correspond well with the observed spectra, the transient absorption is not due to *cis*- or *trans*-**1K**. The TD-DFT-calculated absorption spectrum of the $T_1$ of *cis*-**1K** has major electronic transitions at 305 nm ($f$ = 0.4313), 388 nm ($f$ = 0.1608), and 463 nm ($f$ = 0.3078), which are in excellent agreement with the experimentally observed spectrum (Figure 5). In contrast, the TD-DFT calculations show that the most significant electron transition for the $T_1$ of *trans*-**1K** at longer wavelengths is located at 415 nm ($f$ = 0.2096). Similarly, the TD-DFT-calculated major electronic transitions for the $T_1$ of **1A** and **1B** yield broad spectra between 300 and 600 nm (Figure S1).

To further support the assignment of the observed transient to the $T_1$ of *cis*-**1K**, a kinetic analysis was performed. The transient decays in argon-saturated methanol at 300 and 440 nm were similar, and fitting with a mono-exponential function yielded a rate constant of $8.5 \times 10^4\ s^{-1}$ ($\tau \sim 12\ \mu s$; Figure 6A). It should be noted that the residual absorption did not decay on the microsecond timescale. In oxygen-saturated methanol, the rate constant only increased slightly, whereas the yield of the transient absorbance was smaller, indicating that the precursor ($T_1$ of **1**) to the $T_1$ of *cis*-**1K** is quenched more efficiently by


https://doi.org/10.1021/acs.jpca.3c00543
J. Phys. Chem. A 2023, 127, 2765−2778

**Table 1. Phosphorescence Data and Calculated Energies for the $T_1$ of 1−3 and $T_1$ of 1K−3K**

| | phosphorescence shorter wavelength | | | phosphorescence longer wavelength | | TD-DFT[a](kcal/mol) | |
|---|---|---|---|---|---|---|---|
| compound | (nm) | (kcal/mol) | TD-DFT(kcal/mol) enol | (nm) | (kcal/mol) | *cis*-**K** | *trans*-**K** |
| **1** | 411 | 70 | 70 | 645 | 44 | 51 | 43 |
| **2** | 412 | 69 | 67 | 640 | 45 | 49 | 42 |
| **3** | 411 | 70 | 68 | 651 | 44 | 49 | 42 |

[a]Energies calculated in ethanol using TD-DFT (B3LYP/6-31 + G(d)) with the CPCM for solvation.

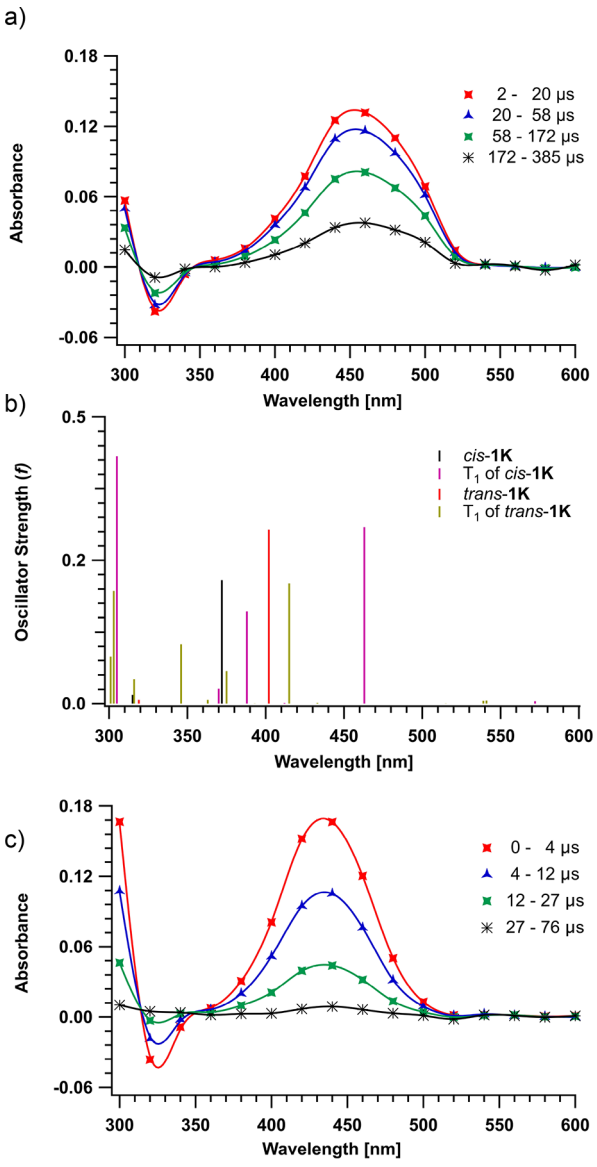


**Figure 5.** Transient spectra obtained by laser flash photolysis (308 nm) of **1** in (a) argon-saturated acetonitrile and (c) argon-saturated methanol. (b) TD-DFT-calculated spectra of the $T_1$ of *trans*-**1K**, $T_1$ of *cis*-**1K**, *trans*-**1K**, and *cis*-**1K** in acetonitrile.

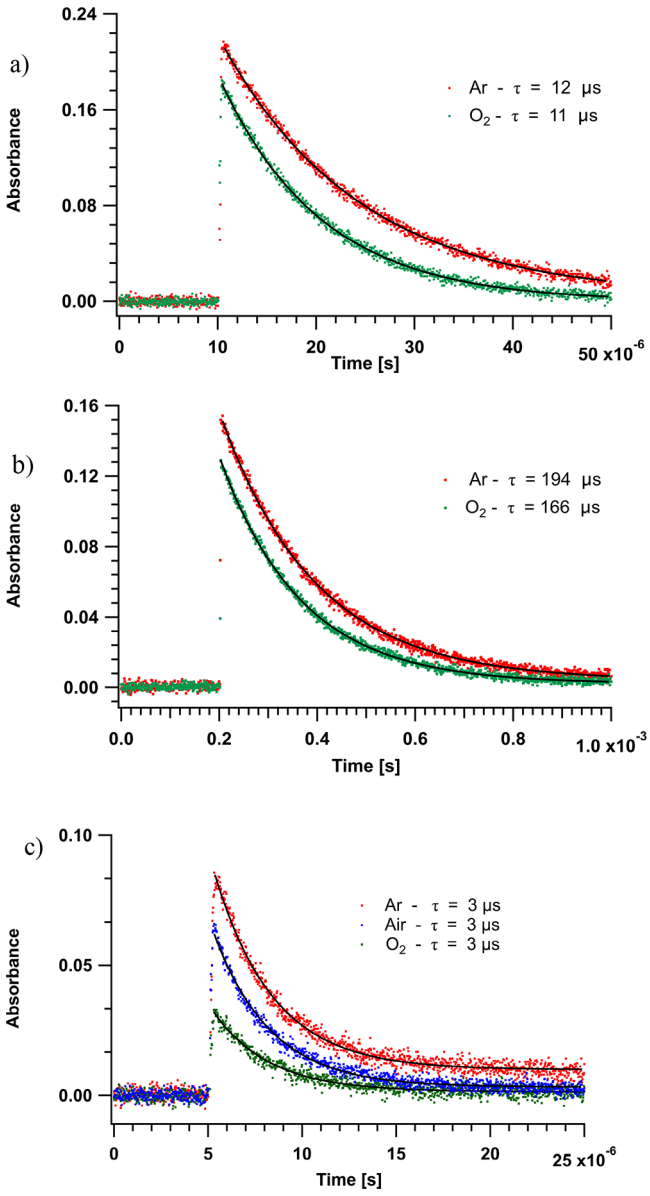


**Figure 6.** Kinetic traces obtained by laser flash photolysis (308 nm) of **1** in argon- and oxygen-saturated (a) methanol at 440 nm, (b) acetonitrile at 460 nm, and (c) in argon-, air-, and oxygen-saturated HMPA at 460 nm.

molecular $O_2$. It is intriguing that the lifetime of the $T_1$ of **1K** is not affected more significantly in oxygen; however, to determine accurately whether it is stable towards oxygen, it would be necessary to form the $T_1$ of **1K** directly from **1K** but not from the excitation of **1**. The rate constant for the decay at 460 nm in HMPA was $3.2 \times 10^5$ $s^{-1}$ ($\tau = 3$ $\mu s$; Figure 6C), and the yield was reduced in oxygen-saturated solution. In contrast, the decay was significantly slower in acetonitrile ($5.1 \times 10^3$ $s^{-1}$, $\tau \sim 190$ $\mu s$; Figure 6B). H-bonding solvents such as methanol and viscous solvents such as HMPA generally impede 1,5-H atom shifts;[46−50] therefore, the observation that the lifetime does not increase in methanol or HMPA supports the assignment of the transient absorption to the $T_1$ of *cis*-**1K** rather than *cis*-**1K**. In addition, as *trans*-**1K** in methanol is stable at ambient



https://doi.org/10.1021/acs.jpca.3c00543
J. Phys. Chem. A 2023, 127, 2765−2778

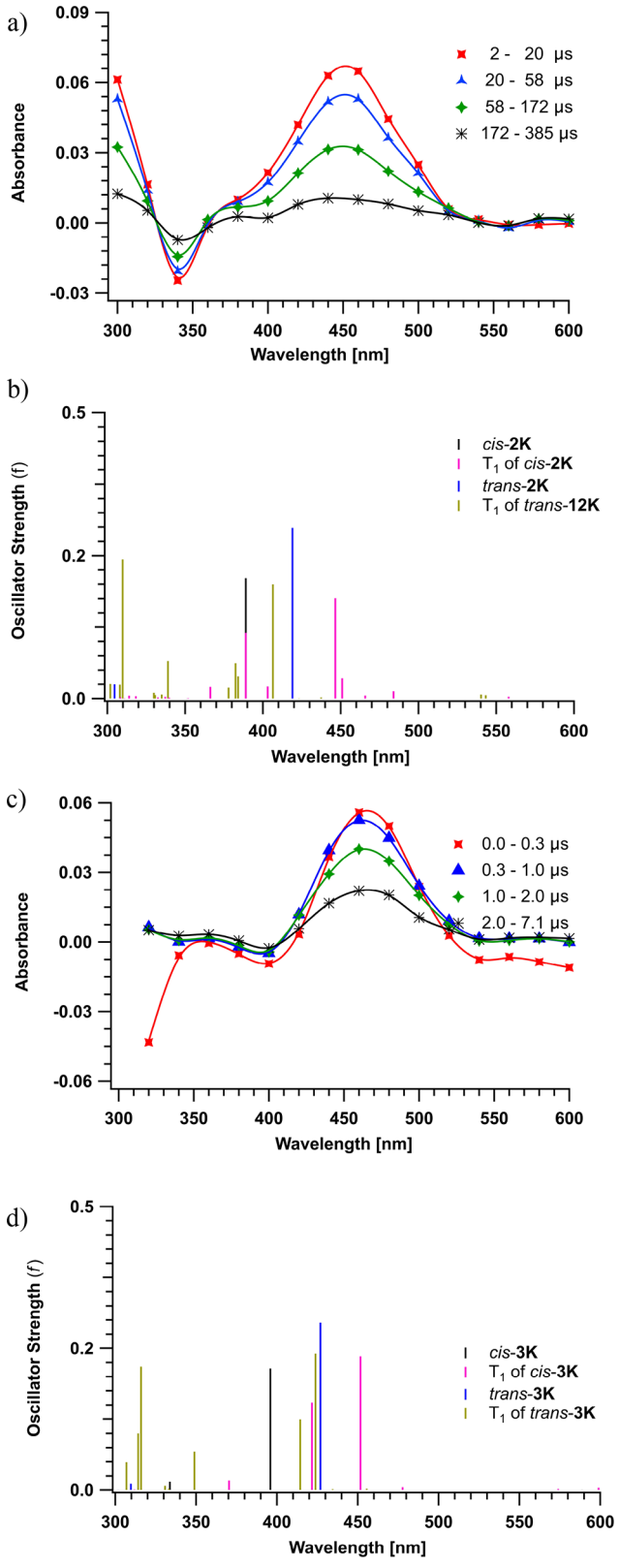


**Figure 7.** Transient spectra obtained by laser flash photolysis (308 nm) of (a) **2** and (c) **3** in argon-saturated methanol. TD-DFT-calculated spectra of (b) the $T_1$ of *trans*-**2K**, $T_1$ of *cis*-**2K**, *trans*-**2K**, and *cis*-**2K** and (d) the $T_1$ of *trans*-**3K**, $T_1$ of *cis*-**3K**, *trans*-**3K**, and *cis*-**3K**. Laser flash photolysis of **2** and **3** in acetonitrile and kinetic traces in methanol and acetonitrile are displayed in Figures S2–S5.

**Table 2. Transient Absorption Lifetimes for the $T_1$ of *cis*-1K–3K in Argon-Saturated Methanol and Acetonitrile**

| | methanol | | acetonitrile | |
|---|---|---|---|---|
| compound | $\lambda_{max}$ (nm) | $\tau$ ($\mu$s) | $\lambda_{max}$ (nm) | $\tau$ ($\mu$s) |
| **1** | 440 | 12 | 460 | 194 |
| **2** | 460 | 151 | 460 | 184 |
| **3** | 460 | 4 | 460 | 13 |

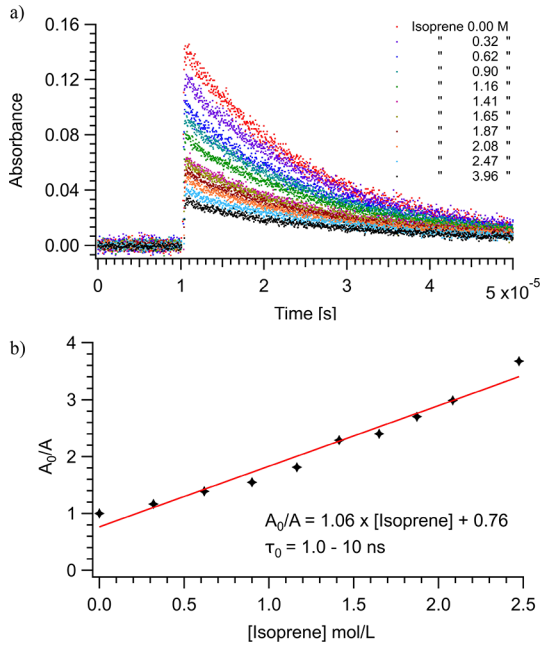


**Figure 8.** (a) Kinetic traces at 440 nm obtained by laser flash photolysis (266 nm) of **1** in argon-saturated methanol with various isoprene concentrations and (b) corresponding Stern–Volmer plot, where $A_0$ and $A$ are the absorption intensities in the absence and presence of isoprene, respectively.

temperature and has an absorption band with a $\lambda_{max}$ at 405 nm, we assigned the residual absorption to *trans*-**1K**.

The transient absorption spectra obtained by laser flash photolysis of **2** and **3** in argon-saturated acetonitrile and methanol were similar to those of **1**, with a $\lambda_{max}$ at 440–460 nm (Figure 7). Furthermore, the observed transients were in excellent agreement with the TD-DFT-calculated spectra of the $T_1$ of *cis*-**2K** and *cis*-**3K**. The $\lambda_{max}$ and lifetimes of the $T_1$ of **1K**–**3K** in various solvents are summarized in Table 2. The lifetime of $T_1$ of *cis*-**2K** is not affected by solvent, as observed for $T_1$ of *cis*-**1K** and $T_1$ of *cis*-**3K**, and thus, we theorize that it is stabilized by both the steric and electron-donating effects of the alkyl substituents and therefore does not show significant solvation effects.

*3.4.1. Quenching Studies and Stern–Volmer Analysis.* To confirm that the $T_1$ of *cis*-**1K** is formed from a triplet precursor (i.e., $T_1$ of **1**) rather than by direct excitation of *trans*-**1K** or *cis*-**1K**, laser flash photolysis (266 nm) of **1** was performed in the presence of isoprene as a triplet quencher. The triplet energy of isoprene has been estimated to be approximately 60 kcal/mol.[51] Therefore, based on the energy levels indicated by the phosphorescence results, isoprene is expected to quench the $T_1$ of **1** but not the $T_1$ of *cis*- or *trans*-**1K**.

The addition of isoprene decreased the absorption intensity, whereas the lifetime of the $T_1$ of *cis*-**1K** was not significantly affected (Figure 7A), indicating that isoprene quenches the



https://doi.org/10.1021/acs.jpca.3c00543
J. Phys. Chem. A 2023, 127, 2765–2778

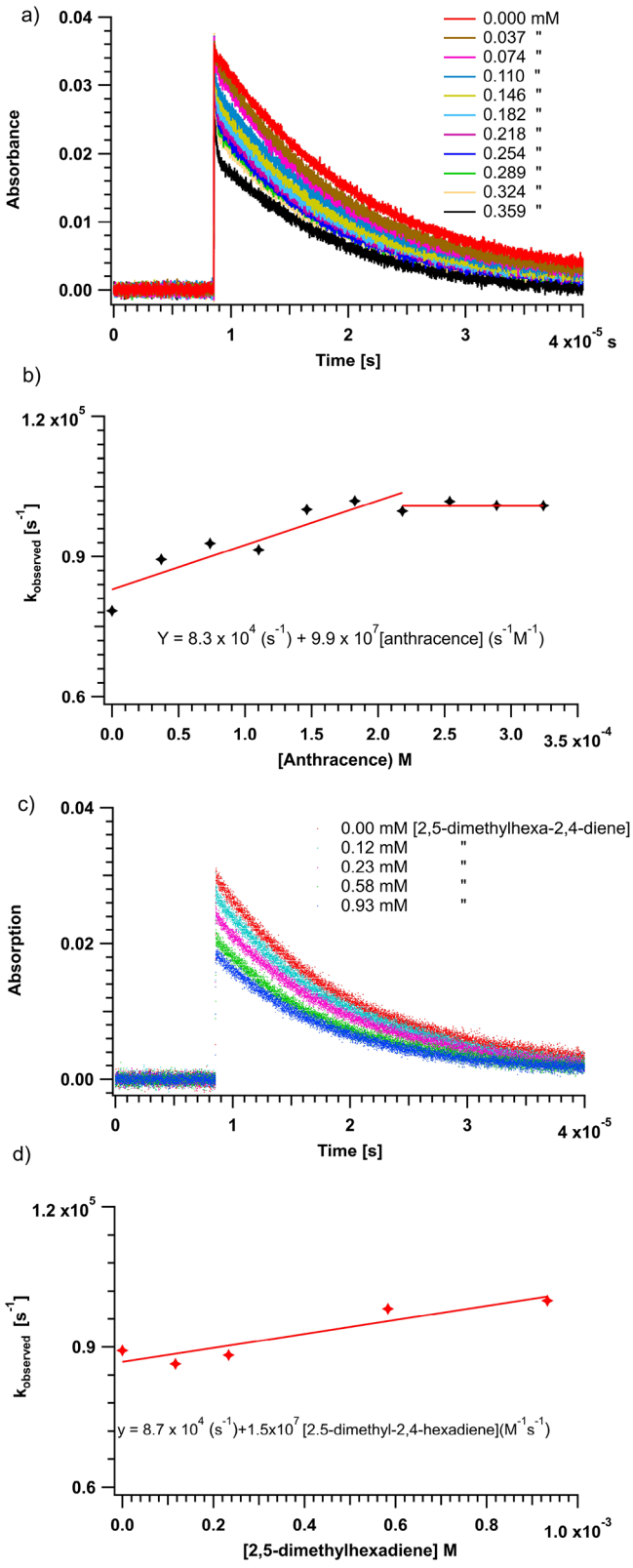


**Figure 9.** (a) Kinetic traces at 440 nm obtained by laser flash photolysis (308 nm) of **1** with various anthracene concentrations and (b) corresponding quenching plot. (c) Kinetic traces at 440 nm with various 2,5-dimethyl-2,4-hexadiene concentrations and (d) corresponding quenching plot.

precursor ($T_1$ of **1**). The Stern–Volmer plot yielded a straight line with a slope of 1.06 $M^{-1}$ (Figure 8). Based on this slope and

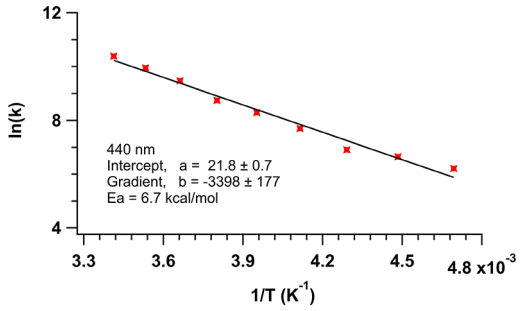


**Figure 10.** Arrhenius plot obtained from the decay of the $T_1$ of *cis*-**1K** in ethanol at 440 nm.

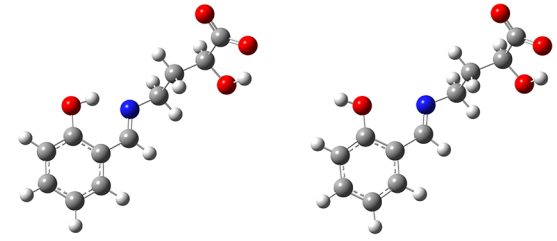


**Figure 11.** Optimized conformers of **1** (B3LYP/6-31 + G(d)).

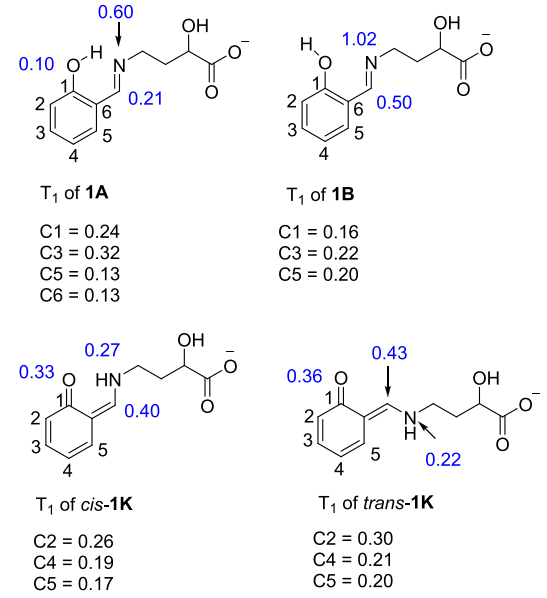


**Figure 12.** Calculated spin densities for optimized $T_1$ of **1A**, $T_1$ of **1B**, $T_1$ of *cis*-**1K**, and $T_1$ of *trans*-**1K** (B3LYP/6-31 + G(d)).

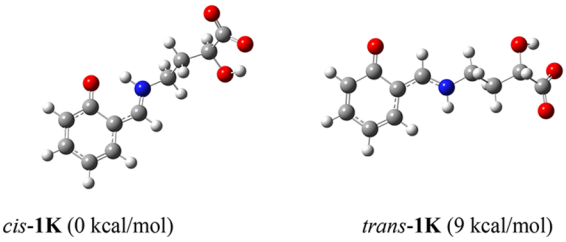


**Figure 13.** Optimized structures of *cis*-**1K** and *trans*-**1K** (B3LYP/6-31 + G(d)).



https://doi.org/10.1021/acs.jpca.3c00543
J. Phys. Chem. A 2023, 127, 2765−2778

**Table 3. Selected Bond Lengths in the Optimized Structures of 1 and $T_1$ of 1 (B3LYP/6-31 + G(d))**

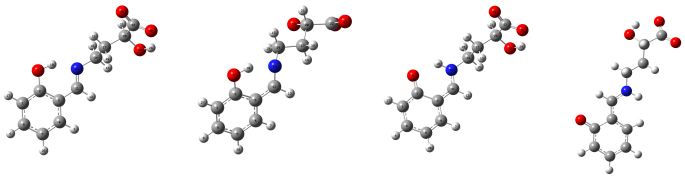

| Bond lengths (Å) | $S_0$ of **1A** | $T_1$ of **1A** | $T_1$ of *cis*-**1K** | $T_1$ of *trans*-**1K** |
|---|---|---|---|---|
| $O_9$–$H_{10}$ | 1.00 | 0.99 | 2.00 | 1.42 |
| $O_9$–$C_2$ | 1.34 | 1.36 | 1.27 | 1.27 |
| $C_2$–$C_1$ | 1.40 | 1.39 | 1.43 | 1.43 |
| $C_4$–$C_3$ | 1.41 | 1.43 | 1.41 | 1.41 |
| $C_3$–$C_2$ | 1.42 | 1.44 | 1.49 | 1.49 |
| $C_{11}$–$N_{13}$ | 1.28 | 1.39 | 1.36 | 1.36 |
| $N_{13}$–$H_{10}$ | 1.72 | 1.80 | 1.02 | 1.01 |

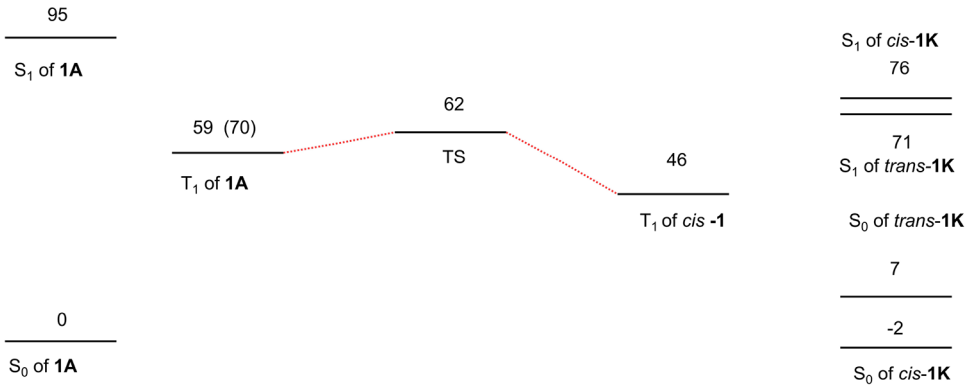


**Figure 14.** Calculated stationary points on the triplet surface of **1**. The calculated energies are in kcal/mol. The energies of the $S_1$ and $T_1$ (70) of **1** and the $S_1$ of *cis*- and *trans*-**1K** were obtained from TD-DFT calculations, whereas the energies of the $S_0$ and $T_1$ (59) of **1**, $S_0$ of *cis*- and *trans*-**1K**, and the transition state (TS) were obtained by optimization using B3LYP/6-31 + G(d).

assuming that the quenching is diffusion controlled ($k_q$ of $10^9$ to $10^{10}$ $M^{-1}$ $s^{-1}$), the lifetime of the $T_1$ of **1** can be estimated as 1.0−10 ns.

Quenching studies were also performed using anthracene, which is a triplet quencher with a lower triplet energy (43 kcal/mol[52]). As observed with isoprene, the addition of anthracene decreased the absorption intensity because the precursor of the $T_1$ of *cis*-**1K** was quenched (Figure 9a). Furthermore, the lifetime of the decay was shortened because anthracene could directly quench the $T_1$ of *cis*-**1K** with a quenching rate constant on the order of $9.9 \times 10^7$ $M^{-1}$ $s^{-1}$. However, the quenching reached a plateau (Figure 9b), indicating that the residual absorption was not quenched and thus can be attributed to *trans*-**1K**. As fluorescence from anthracene interfered with the decay on shorter timescales, we also used 2,5-dimethyl-2,4-hexadiene as a quencher, which has an estimated triplet energy of 42 kcal/mol.[31] As expected, both the $T_1$ of **1** and the $T_1$ of *cis*-**1K** were quenched (Figure 9c), and the quenching rate constant for the $T_1$ of *cis*-**1K** with 2,5-dimethyl-2,4-hexadiene was $1.5 \times 10^7$ $M^{-1}$ $s^{-1}$ (Figure 9d), which is comparable to that with anthracene. Thus, the quenching studies provide additional support to the hypothesis that the transient absorption is mainly due to the $T_1$ of *cis*-**1K** as well as a small amount of *trans*-**1K**.

*3.4.2. Arrhenius Plots.* To determine the activation barrier for the decay of the transient absorption, temperature-dependent laser flash photolysis experiments (266 nm) were performed in ethanol. Based on the kinetic traces at 440 nm, the lifetime of the $T_1$ of *cis*-**1K** increased as the temperature decreased from 293 to 173 K. The Arrhenius equation gives the dependence of the rate constant $k$ of a chemical reaction on the absolute temperature $T$ (K), where $A$ is the pre-exponential factor, $E_a$ is the activation energy, and $R$ is the universal gas constant:

$$k = Ae^{-E_a/RT}$$

Thus, by plotting $\ln(k_{observed})$ versus $1/T$, the activation energy can be determined from the slope. The activation energies determined from the kinetics at 440 nm was 6.7 kcal/mol (Figure 10). We assigned the measured activation energy to the barrier for intersystem crossing from the $T_1$ of *cis*-**1K** to *cis*-**1K**, that is, the rotation required to obtain a conformer of the $T_1$ of *cis*-**1K** that can undergo intersystem crossing.

**3.5. Calculations.** We performed DFT calculations to support the formation mechanism for the $T_1$ of **1K**−**3K** and **1K**−**3K** from **1**−**3** and to verify the suggestion that the rate-determining step is the intersystem crossing of the $T_1$ of **K** to form *cis*-**K** as *cis*-**K** undergoes an efficient 1,5-H atom shift to regenerate **1**−**3**. All the structures were optimized using Gaussian16 at the B3LYP level of theory with the 6-31 + G(d) basis set.[26,28,44]

The optimized ground state ($S_0$) of **1** has several minimal energy conformers (Figure 11). Conformer **1A**, which is the minimum energy conformer, has an intramolecular hydrogen bond between Ph-OH and the imine moiety. There are several other conformers with intramolecular hydrogen bonds because the alkyl side chain of **1** is flexible. Conformer **1B**, which does not have an intramolecular hydrogen bond, is 18 kcal/mol less


https://doi.org/10.1021/acs.jpca.3c00543
J. Phys. Chem. A 2023, 127, 2765−2778

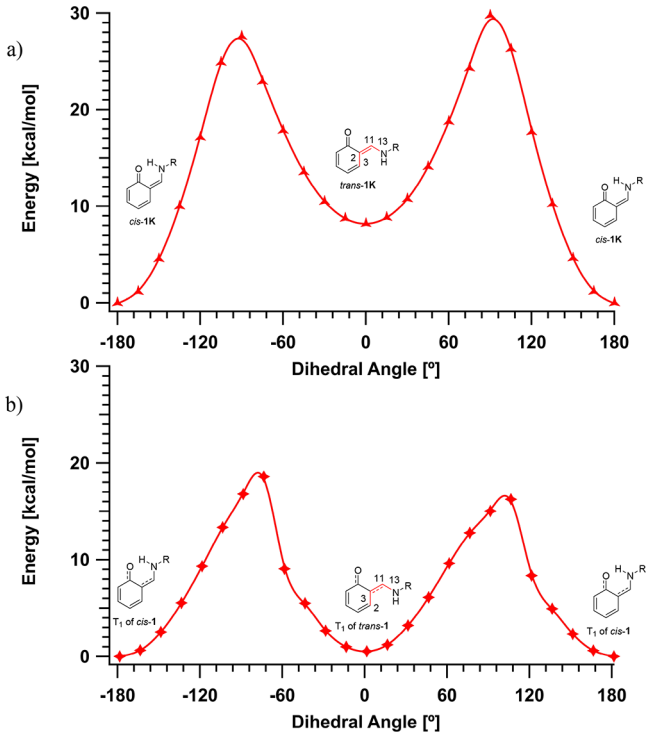


**Figure 15.** Calculated (B3LYP/6-31 + G(d)) rotational barriers around the $C_2-C_3-C_{11}-N_{13}$ dihedral angles of (a) *cis*-**1K** and (b) $T_1$ of *cis*-**1K**. Note that *cis*-**1K** and the $T_1$ of *cis*-**1K** are not flat and, therefore, the curves are not symmetrical.

**Scheme 4. 1,5-H atom shift to regenerate 1 from *cis*-1K**

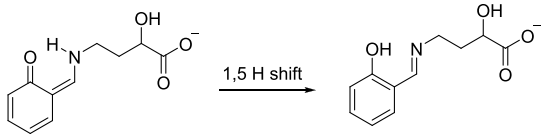


**Table 4. Calculated Transition State Barriers for Regenerating 1−3 through a 1,5-H Atom Shift**

| calculated transition state barrier for 1,5-H atom shift (kcal/mol)[a] | B3LYP/6-31 + G(d) | B3LYP-D3/def2-TZVP[b] | DLPNO-CCSD(T)/CBS[b] | M062X | MP2 |
|---|---|---|---|---|---|
| *cis*-**1K** | 2.4 | 1.7 | 4.3 | 0.7 | 0.4 |
| *cis*-**2K** | 2.5 | | | | |
| *cis*-**3K** | 3.3 | | | | |

[a]With zero-point energy corrections. [b]Methanol solvation.

**Table 5. Relative Energies (kcal/mol) of *cis*-1K, *trans*-1K, and 1 Calculated Using the CPCM for Solvation in Acetonitrile**

| method | *cis*-**1K** | *trans*-**1K** | **1** |
|---|---|---|---|
| B3LYP-D3BJ/def2-TZVP | 0 | 5.6 | 1.1 |
| DLPNO-CCSD(T)/CBS | 2.2 | 7.7 | 0 |

stable than conformer **1A**, highlighting the importance of intramolecular hydrogen bonding for stabilizing **1** in the gas phase. However, in solvents such as methanol, intermolecular hydrogen bonding with the solvent molecules is expected to stabilize conformers that do not have intramolecular hydrogen bonds.

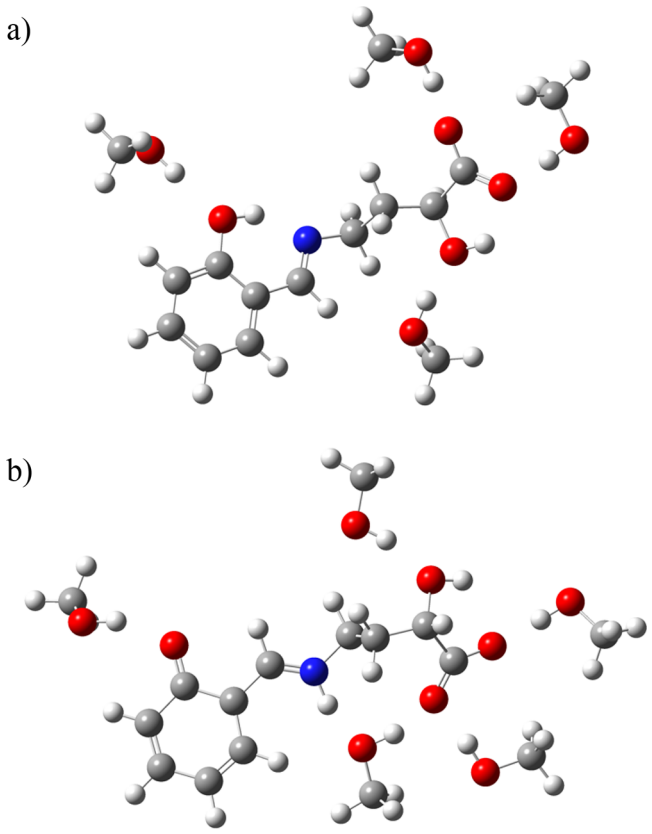


**Figure 16.** (a) **1** and (b) *trans*-**1K** with attached solvent (methanol) molecules.

TD-DFT calculations using CPCM for solvation in acetonitrile located the first excited singlet state ($S_1$) of **1A** at 95 kcal/mol and the $T_1$ of **1A** at 70 kcal/mol above the $S_0$. We also optimized the $T_1$ of **1A** and found that it is located 59 kcal/mol above its $S_0$. Similarly, TD-DFT calculations located the $S_1$ of **1B** at 100 kcal/mol and the $T_1$ of **1B** at 72 kcal/mol above the $S_0$, whereas the optimized structure was 49 kcal/mol above the $S_0$ of **1B**. Spin density calculations demonstrated that the unpaired spin is mainly localized on the N atom, with a smaller amount on the C=N carbon atom and the phenyl group (Figure 12). Thus, the spin density calculations indicate that the $T_1$ of **1** has an $(n,\pi^*)$ configuration, which is consistent with the phosphorescence results. It is well documented that B3LYP underestimates the energies of triplets with $(n,\pi^*)$ configurations;[53] thus, it is reasonable that the energies obtained by optimization were lower than those obtained from the TD-DFT calculations.

The optimized $S_0$ of *cis*-**1K** and *trans*-**1K** were located at −2 and 7 kcal/mol relative to the $S_0$ of **1A** (Figure 13). Thus, although *cis*-**1K** is stabilized by intermolecular hydrogen bonding, the energy difference between the tautomers with and without intramolecular hydrogen bonding is less than that between **1A** and **1B**, presumably because of the steric demand of the *cis* alignment, which is also reflected by the intramolecular hydrogen bond being longer in *cis*-**1K** than in **1A** (Table 3). For *cis*-**1K** and *trans*-**1K**, TD-DFT calculations located the $S_1$ at 76 and 71 kcal/mol, respectively, and the $T_1$ at 51 and 43 kcal/mol, respectively, above the $S_0$.

The optimized structures of the $T_1$ of *cis*-**1K** and the $T_1$ of *trans*-**1K** are both located at 46 kcal/mol above the $S_0$ of **1**. These calculations imply that intramolecular hydrogen bonding



https://doi.org/10.1021/acs.jpca.3c00543
J. Phys. Chem. A 2023, 127, 2765−2778

**Scheme 5. ESIPT on the Triplet Surface of $T_1$ of 1 to Form *cis*- and *trans*-1K**

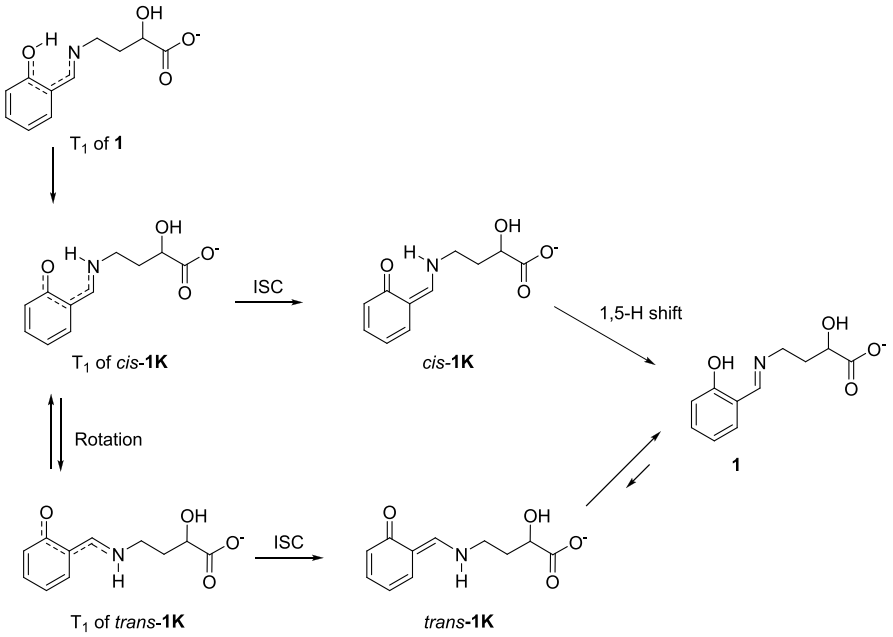


**Scheme 6. Photoenolization of *o*-Methyl Aryl Ketones**

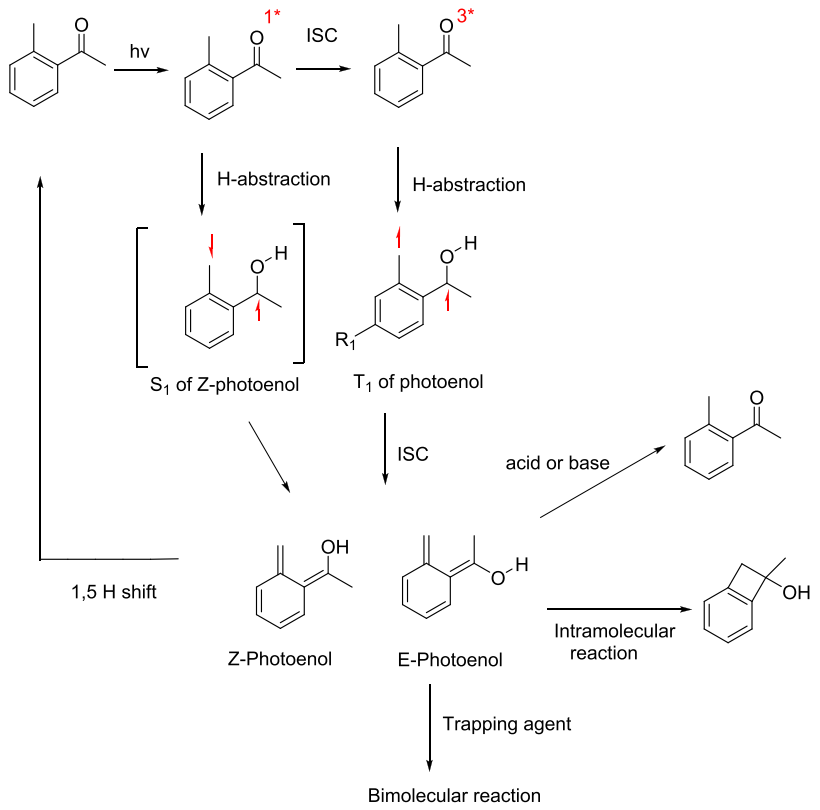


is significantly weaker in the $T_1$ of *cis*-**1K** than in **1A** and *cis*-**1K**, as further highlighted by the hydrogen bond length of 1.99 Å. Spin density calculations showed that the unpaired electrons in the $T_1$ of *cis*- and *trans*-**1K** are delocalized over the keto C═O group, the imine moiety, and the aromatic ring.

The calculated stationary points on the triplet surface of **1** for the formation of the $T_1$ of **1K**, *cis*-**1K**, and *trans*-**1K** are displayed in Figure 14. The transition state for intramolecular H-atom abstraction in $T_1$ of **1** to form the $T_1$ of **1K** was located 62 kcal/mol above the $S_0$ of **1**; hence, the transition state barrier to form the $T_1$ of *cis*-**1K** is ∼3 kcal/mol. It should be noted that optimized structure of $S_0$ of *cis*-**1K** is 1.57 kcal/mol more stable than $S_0$ of **1A**; however, the energy difference is within uncertainty of the calculations.

We calculated the rotational barriers for rotation around the $C_2-C_3-C_{11}-N_{13}$ dihedral angle of *cis*-**1K** and the $T_1$ of *cis*-**1K** (Figure 15). For the $T_1$ of *cis*-**1K**, the maximum rotational barrier was 19 kcal/mol, which corresponds to breaking of the



https://doi.org/10.1021/acs.jpca.3c00543
J. Phys. Chem. A 2023, 127, 2765−2778

intramolecular hydrogen bond. The rotational barrier for *cis*-**1K** was considerably higher (29 kcal/mol), indicating that rotation in the triplet excited state is more efficient than in the ground state.

Finally, we calculated the transition state of *cis*-**1K** to regenerate **1** through a 1,5-H atom shift (Scheme 4). The B3LYP/6-31 + G(d) calculation located the transition state at 2.4 kcal/mol (with zero point energy correction). Although this energy is lower than the measured activation barrier for the decay of the $T_1$ of *cis*-**1K**, which is consistent with the decay being due to intersystem crossing, it is within the estimated error of the calculations. We attempted to use different theories and basis sets to improve the accuracy of the transition state barrier calculation (Table 4). The M062X/6-31 + G(d) calculation placed the transition state barrier for *cis*-**1K** at 0.7 kcal/mol above the $S_0$ of **1**, whereas MP2 placed the transition state at 0.4 kcal/mol.

Similar to the correlation-consistent composite approach,[54,55] DLPNO-CCSD(T)/CBS single-point energy calculations were carried out for structures optimized using the B3LYP[56]/def2-TZVP[57] method. B3LYP/def2-TZVP zero-point energies and Grimme dispersion corrections[56] with Becke−Johnson damping[58] were used. The extrapolation of the DLPNO-CCSD(T) energies to the complete basis set was performed as follows: $E_{\mathrm{HF}}^{\mathrm{CBS}} = \frac{E(n_1)n_1^3 - E(n_2)n_2^3}{n_1^3 - n_2^3}$ for the Hartree−Fock energy,[59] and $E_{\mathrm{corr}}^{\mathrm{CBS}} = \frac{X^\beta E_{\mathrm{corr}}^{(X)} - Y^\beta E_{\mathrm{corr}}^{(Y)}}{X^\beta - Y^\beta}$ for the correlation energy[60] using $\beta = 3.05$ as advised in the ORCA 4.2.1 reference manual.[57,58] Augmented triple- and quadruple-exponent correlation-consistent basis sets[61] were used in conjunction with the corresponding auxiliary sets[62] supplied with ORCA 4.2.1.[57,58]

Thus, our approach demonstrates that the 1,5-H atom shift is nearly barrierless as the barrier height is comparable to the intrinsic approximation error of the DFT or DLPNO-CCSD(T)/CBS methods. Furthermore, the calculated transition state barrier for the $T_1$ of *cis*-**1K** to reform **1** is on the same order as those reported by Ortiz-Sanchez et al. and Spörkel et al. for the *cis*-keto tautomer of salicylideneaniline.[23,63]

Furthermore, coupled cluster calculations (Table 5) indicated that **1** is 2.2 kcal/mol more stable than *cis*-**1K**, which makes the enol form more favorable in solution. Although the calculations show that *trans*-**1K** is higher in energy than **1**, we theorize that *trans*-**1K** is better stabilized by solvents because it has an additional hydrogen bonding site (Figure 16).

## 4. DISCUSSION

The photolysis of **1**−**3** results in intramolecular H-atom abstraction on the triplet surface to form the $T_1$ of the corresponding *cis*-**K** (Scheme 5). The $T_1$ of *cis*-**K** presumably intersystem crosses to *cis*-**K**, but the rate of intersystem crossing is slower than the rate of the 1,5-H atom shift; thus, *cis*-**K** is not observed by laser flash photolysis. Similarly, it can be theorized that the $T_1$ of *cis*-**K** can rotate and intersystem-cross to form *trans*-**K**, although *trans*-**K** can also be formed via the singlet reactivity of **1**−**3**. The substituents on the phenol ring in **1**−**3** do not significantly affect their photochemistry or keto tautomerization. However, it can be theorized that the $T_1$ of *cis*-**3K** decays more efficiently because chlorine as a heavy atom promotes intersystem crossing.

The phototautomerization of **1**−**3** is similar to that of *ortho*-hydroxyacetophenone derivatives, which undergo phototautomerization on the triplet surface upon direct irradiation.[64] In addition, the phototautomerization of **1**−**3** shows some similarity to the photoenolization of *o*-alkyl-substituted arylketones (Scheme 6).[46,65] Intramolecular H-atom abstraction on the single surface of *o*-alkyl aryl ketones yields the corresponding *cis*-photoenols, which are short-lived and reform the starting material through an efficient 1,5-H atom shift. In comparison, H-atom abstraction on the triplet surface generally yields biradicals that intersystem cross to yield both *cis*- and *trans*-photoenols. It should be noted that these triplet biradicals can also be referred to as the triplet excited states of the photoenols. Because *trans*-photoenols are long-lived, they have various applications in synthesis and as photoremovable protecting groups.[66,67]

**Scheme 7. Photoenolization of 5 and 6**

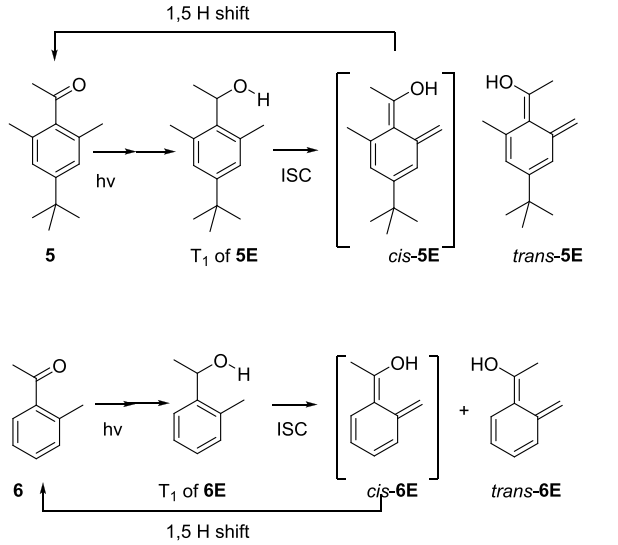


Furthermore, the intersystem crossing of the triplet excited state of some photoenol derivatives has been reported to be slower than the 1,5-H atom shift of the corresponding *cis*-photoenols. In detail, the triplet excited states of *cis*- and *trans*-photoenols ($T_1$ of **5E** and **6E**), formed by intramolecular H-atom abstraction in ketones **5** and **6**, are longer-lived than the corresponding *cis*-photoenols (*cis*-**5E** and *cis*-**6E**), which decay through an efficient 1,5-H atom shift (Scheme 7). Laser flash photolysis of ketones **5** and **6** allows for the direct detection of *trans*-**5E** and *trans*-**6E** but not *cis*-**5E** and *cis*-**6E** in solvents such as methanol and acetonitrile.[47] However, in more viscous HMPA, the 1,5-H atom shift in *cis*-**5E** and *cis*-**6E** becomes slower than the intersystem crossing of the $T_1$ of **5E** and **6E**. For the $T_1$ of **5E**, the activation barrier for intersystem crossing was measured to be 4.7 kcal/mol, which is on the same order as that for the $T_1$ of *cis*-**1K**.

Finally, the transient absorption obtained by laser flash photolysis of **1**−**3** on nanosecond timescales is similar to that reported for Schiff base derivatives[68] in terms of both absorption maxima and lifetimes. These transients were assigned to twisted enols as they are not quenched by molecular oxygen; however, because the absorption of the $T_1$ of **1K** is directly quenched by triplet quenchers, it does not correspond to a twisted conformer of **1**.

## 5. CONCLUSIONS

Upon irradiation, **1**−**3** form the corresponding $T_1$, which undergoes efficient intramolecular H atom transfer to form the $T_1$ of *cis*-**K**. The $T_1$ of **K** decays by intersystem crossing to mainly



https://doi.org/10.1021/acs.jpca.3c00543
J. Phys. Chem. A 2023, 127, 2765−2778

form *cis*-**K**, which cannot be detected directly because an efficient 1,5-H atom shift occurs to reform **1**−**3**. The $T_1$ of *cis*-**1K** is not quenched efficiently by molecular oxygen, but its triplet character was verified by quenching studies with triplet quenchers. Thus, Schiff bases, such as **1**−**3**, have the potential to be used as triplet sensitizers or photocatalysts, although it is still not well-established which Schiff bases undergo ESPIT on their triplet excited state.

## ■ ASSOCIATED CONTENT

### Supporting Information

The Supporting Information is available free of charge at https://pubs.acs.org/doi/10.1021/acs.jpca.3c00543.

Cartesian coordinates, energies, vibrational frequencies of **1**−**3**, and NMR spectra of **1**−**3** (PDF)

## ■ AUTHOR INFORMATION


### Corresponding Author

**Anna D. Gudmundsdottir** − *Department of Chemistry, University of Cincinnati, Cincinnati, Ohio 45221-0172, United States;* orcid.org/0000-0002-5420-4098; Email: anna.gudmundsdottir@uc.edu

### Authors

**Geethika K. Weragoda** − *Department of Chemistry, University of Cincinnati, Cincinnati, Ohio 45221-0172, United States*

**Nayera M. Abdelaziz** − *Department of Chemistry, University of Cincinnati, Cincinnati, Ohio 45221-0172, United States*

**Dmitrii Govorov** − *Department of Chemistry, University of Cincinnati, Cincinnati, Ohio 45221-0172, United States*

**Rajkumar Merugu** − *Department of Chemistry, University of Cincinnati, Cincinnati, Ohio 45221-0172, United States*

**Leanna J. Patton** − *Department of Chemistry, University of Cincinnati, Cincinnati, Ohio 45221-0172, United States;* orcid.org/0000-0001-6464-8760

**Jennifer E. Grabo** − *Department of Chemistry, University of Cincinnati, Cincinnati, Ohio 45221-0172, United States*

**R. A. A. Upul Ranaweera** − *Department of Chemistry, University of Cincinnati, Cincinnati, Ohio 45221-0172, United States;* orcid.org/0000-0003-1614-1919

**Anna C. Ratliff** − *Department of Chemistry, University of Cincinnati, Cincinnati, Ohio 45221-0172, United States*

**W. Dinindu Mendis** − *Department of Chemistry, University of Cincinnati, Cincinnati, Ohio 45221-0172, United States*

**Noha Ahmed** − *Department of Chemistry, University of Cincinnati, Cincinnati, Ohio 45221-0172, United States*

**Katrin H. Vilinsky** − *Department of Chemistry, University of Cincinnati, Cincinnati, Ohio 45221-0172, United States*

**Manabu Abe** − *Department of Chemistry, Graduate School of Advanced Science and Engineering and International Institute for Sustainability with Knotted Chiral Meta Matter (WPI-SKCM2), Hiroshima University, Higashi-Hiroshima, Hiroshima 739-8526, Japan;* orcid.org/0000-0002-2013-4394

**Michael J. Baldwin** − *Department of Chemistry, University of Cincinnati, Cincinnati, Ohio 45221-0172, United States;* orcid.org/0000-0001-9912-9717

Complete contact information is available at: https://pubs.acs.org/10.1021/acs.jpca.3c00543


### Author Contributions

[⊥]D.G., R.M., L.J.P., and J.E.G. contributed equally to this work.

### Notes

The authors declare no competing financial interest.

## ■ ACKNOWLEDGMENTS

We thank the NSF (CHE-2102248 and CHE-1156449) and OSC (PES0597) for support. G.K.W. and R.M. thank UC for URC fellowships, D.G. is grateful for Doctoral Enhancement Fellowship from the Chemistry Department, and N.M.A. acknowledges the Chemistry Department for Doctoral Enhancement and H. Brian Halsall fellowships. A.C.R. acknowledges NSF-REU fellowships (CHE-1156449). M.A. gratefully acknowledges financial support from JSPS KAKENHI (grant no. JP17H03022).

## ■ REFERENCES


(1) Weller, A. Intramolecular Proton Transfer in Excited States. *Z. Elektrochem. Angew. Phys. Chem.* **1956**, *60*, 1144−1147.

(2) Barbara, P. F.; Rentzepis, P. M.; Brus, L. E. Photochemical Kinetics of Salicylidenaniline. *J. Am. Chem. Soc.* **1980**, *102*, 2786−2791.

(3) Okabe, C.; Nakabayashi, T.; Inokuchi, Y.; Nishi, N.; Sekiya, H. Ultrafast Excited-State Dynamics in Photochromic N-Salicylideneaniline Studied by Femtosecond Time-Resolved Rempi Spectroscopy. *J. Chem. Phys.* **2004**, *121*, 9436−9442.

(4) Kandappa, S. K.; Valloli, L. K.; Ahuja, S.; Parthiban, J.; Sivaguru, J. Taming the Excited State Reactivity of Imines − from Non-Radiative Decay to Aza Paternò−Büchi Reaction. *Chem. Soc. Rev.* **2021**, *50*, 1617−1641.

(5) Exelby, R.; Grinter, R. Phototropy (or Photochromism). *Chem. Rev.* **1965**, *65*, 247−260.

(6) Nakatani, K.; Delaire, J. A. Reversible Photoswitching of Second-Order Nonlinear Optical Properties in an Organic Photochromic Crystal. *Chem. Mater.* **1997**, *9*, 2682−2684.

(7) Zaichenko, N. L.; Shienok, A. I.; Koltsova, L. S.; Mardaleishvili, I. R.; Tatikolov, A. S.; Levin, P. P.; Berlin, A. A. Bifunctional Photosensitive Compound for Optical Processors. *Physica Status Solidi C* **2011**, *8*, 2746−2748.

(8) Levin, P. P.; Tatikolov, A. S.; Zaichenko, N. L.; Shienok, A. I.; Kol'tsova, L. S.; Mardaleishvili, I. R.; Popov, L. D.; Levchenkov, S. I.; Berlin, A. A. Study of Spectral and Kinetic Characteristics of Products of Photolysis of a Trifunctional Compound with Light of Different Wavelengths. *High Energy Chem.* **2012**, *46*, 259−265.

(9) Rodriguez-Prieto, M. F.; Nickel, B.; Grellmann, K. H.; Mordzinski, A. Dual Phosphorescence from 2-(2'-Hydroxyphenyl)Benzoxazole Due to Keto-Enol Tautomerism in the Metastable Triplet State. *Chem. Phys. Lett.* **1988**, *146*, 387−392.

(10) Brewer, W. E.; Martinez, M. L.; Chou, P.-T. Mechanism of the Ground-State Reverse Proton Transfer of 2-(2-Hydroxyphenyl)-Benzothiazole. *J. Phys. Chem.* **1990**, *94*, 1915−1918.

(11) Al-Soufi, W.; Grellmann, K. H.; Nickel, B. Keto-Enol Tautomerization of 2-(2'-Hydroxyphenyl)Benzoxazole and 2-(2'-Hydroxy-4′-Methylphenyl)Benzoxazole in the Triplet State: Hydrogen Tunneling and Isotope Effects. Transient Absorption Kinetics. *J. Phys. Chem.* **1991**, *95*, 10503−10509.

(12) Hoshimoto, E.; Yamauchi, S.; Hirota, N.; Nagaoka, S. Investigation of Proton-Transferred Enol Tautomers in the Lowest Excited Triplet States of Methyl Salicylate and Related Molecules. *J. Phys. Chem.* **1991**, *95*, 10229−10235.

(13) Chou, P. T.; Studer, S. L.; Martinez, M. L. Studies of the Triplet State of 2-(2'-Hydroxyphenyl) Benzothiazole. *Chem. Phys. Lett.* **1991**, *178*, 393−398.

(14) Stephan, J. S.; Mordzinski, A.; Rodriguez, C. R.; Grellmann, K. H. Photoisomerizations of the Photochromic Anil Salicylidene-1-Naphthylamine in 3-Methylpentane. *Chem. Phys. Lett.* **1994**, *229*, 541−550.

(15) Tokumura, K.; Kurauchi, M.; Yagata, N.; Itoh, M. Phototautomerization of 3-Hydroxyflavone in the Lowest Triplet State. *Chem. Phys. Lett.* **1996**, *258*, 495−500.

(16) Nagaoka, S.; Yamamoto, S.; Mukai, K. Intramolecular Proton Transfer in the Triplet State of 1-(Acylamino)Anthraquinones. *J. Photochem. Photobiol., A* **1997**, *105*, 29−33.
(17) Catalán, J.; Diaz, C. Induction of Triplet-State Emission of the Transient Proton-Transfer Keto Form of Methyl Salicylate by Heavy-Atom Perturbation. *J. Phys. Chem. A* **1998**, *102*, 323−328.
(18) Ziolek, M.; Kubicki, J.; Maciejewski, A.; Naskrecki, R.; Grabowska, A. Excited State Proton Transfer and Photochromism of an Aromatic Schiff Base. Pico- and Femtosecond Kinetics of the N,N'-Bis(Salicylidene)-p-Phenylenediamine (BSP). *Chem. Phys. Lett.* **2003**, *369*, 80−89.
(19) Fukuda, H.; Amimoto, K.; Koyama, H.; Kawato, T. Crystalline Photochromism of N-Salicylidene-2,6-Dialkylanilines: Advantage of 2,6-Dialkyl Substituents of Aniline for Preparation of Photochromic Schiff Base Crystals. *Org. Biomol. Chem.* **2003**, *1*, 1578−1583.
(20) Fita, P.; Luzina, E.; Dziembowska, T.; Kopeć, D.; Piątkowski, P.; Radzewicz, C.; Grabowska, A. Keto-Enol Tautomerism of Two Structurally Related Schiff Bases: Direct and Indirect Way of Creation of the Excited Keto Tautomer. *Chem. Phys. Lett.* **2005**, *416*, 305−310.
(21) Rodriguez-Cordoba, W.; Zugazagoitia, J. S.; Collado-Fregoso, E.; Peon, J. Excited State Intramolecular Proton Transfer in Schiff Bases. Decay of the Locally Excited Enol State Observed by Femtosecond Resolved Fluorescence. *J. Phys. Chem. A* **2007**, *111*, 6241−6247.
(22) Jankowska, J.; Rode, M. F.; Sadlej, J.; Sobolewski, A. L. Photophysics of Schiff Bases: Theoretical Study of Salicylidene Methylamine. *ChemPhysChem* **2012**, *13*, 4287−4294.
(23) Sporkel, L.; Cui, G.; Thiel, W. Photodynamics of Schiff Base Salicylideneaniline: Trajectory Surface-Hopping Simulations. *J. Phys. Chem. A* **2013**, *117*, 4574−4583.
(24) Pfund, B.; Steffen, D. M.; Schreier, M. R.; Bertrams, M.-S.; Ye, C.; Börjesson, K.; Wenger, O. S.; Kerzig, C. UV Light Generation and Challenging Photoreactions Enabled by Upconversion in Water. *J. Am. Chem. Soc.* **2020**, *142*, 10468−10476.
(25) Becke, A. D. Density-functional Exchange-Energy Approximation with Correct Asymptotic Behavior. *Phys. Rev. A* **1988**, *38*, 3098.
(26) Lee, C.; Yang, W.; Parr, R. G. Development of the Colle-Salvetti Correlation-Energy Formula into a Functional of the Electron Density. *Phys. Rev. B: Condens. Matter* **1988**, *37*, 785−789.
(27) Zhao, Y.; Truhlar, D. G. The M06 Suite of Density Functionals for Main Group Thermochemistry, Thermochemical Kinetics, Noncovalent Interactions, Excited States, and Transition Elements: Two New Functionals and Systematic Testing of Four M06-Class Functionals and 12 Other Functionals. *Theor. Chem. Acc.* **2008**, *120*, 215−241.
(28) Frisch, M. J.; Trucks, G. W.; Schlegel, H. B.; Scuseria, G. E.; Robb, M. A.; Cheeseman, J. R.; Scalmani, G.; Barone, V.; Petersson, G. A.; Nakatsuji, H., et al. *Gaussian 16 Rev. C.01*, Wallingford, CT, 2016.
(29) Gonzalez, C.; Schlegel, H. B. An Improved Algorithm for Reaction Path Following. *J. Chem. Phys.* **1989**, *90*, 2154−2161.
(30) Gonzalez, C.; Schlegel, H. B. Reaction Path Following in Mass-Weighted Internal Coordinates. *J. Phys. Chem.* **1990**, *94*, 5523−5527.
(31) Foresman, J. B.; Head-Gordon, M.; Pople, J. A.; Frisch, M. J. Toward a Systematic Molecular Orbital Theory for Excited States. *J. Phys. Chem.* **1992**, *96*, 135−149.
(32) Bauernschmitt, R.; Ahlrichs, R. Treatment of Electronic Excitations within the Adiabatic Approximation of Time Dependent Density Functional Theory. *Chem. Phys. Lett.* **1996**, *256*, 454−464.
(33) Stratmann, R. E.; Scuseria, G. E.; Frisch, M. J. An Efficient Implementation of Time-Dependent Density-Functional Theory for the Calculation of Excitation Energies of Large Molecules. *J. Chem. Phys.* **1998**, *109*, 8218−8224.
(34) Klamt, A.; Schüürmann, G. Cosmo: A New Approach to Dielectric Screening in Solvents with Explicit Expressions for the Screening Energy and Its Gradient. *J. Chem. Soc. Perkin Trans.* **1993**, *2*, 799−805.
(35) Takano, Y.; Houk, K. N. Benchmarking the Conductor-Like Polarizable Continuum Model (CPCM) for Aqueous Solvation Free Energies of Neutral and Ionic Organic Molecules. *J. Chem. Theory Comput.* **2005**, *1*, 70−77.
(36) Liakos, D. G.; Guo, Y.; Neese, F. Comprehensive Benchmark Results for the Domain Based Local Pair Natural Orbital Coupled Cluster Method (DLPNO-CCSD(T)) for Closed- and Open-Shell Systems. *J. Phys. Chem. A* **2020**, *124*, 90−100.
(37) Neese, F. The ORCA Program System. *WIREs Comput. Mol. Sci.* **2012**, *2*, 73−78.
(38) Neese, F. Software Update: The ORCA Program System, Version 4.0. *WIREs Comput. Mol. Sci.* **2018**, *8*, No. e1327.
(39) Barone, V.; Cossi, M. Quantum Calculation of Molecular Energies and Energy Gradients in Solution by a Conductor Solvent Model. *J. Phys. Chem. A* **1998**, *102*, 1995−2001.
(40) Cossi, M.; Rega, N.; Scalmani, G.; Barone, V. Energies, Structures, and Electronic Properties of Molecules in Solution with the C-PCM Solvation Model. *J. Comput. Chem.* **2003**, *24*, 669−681.
(41) Muthukrishnan, S.; Sankaranarayanan, J.; Klima, R. F.; Pace, T. C. S.; Bohne, C.; Gudmundsdottir, A. D. Intramolecular H-Atom Abstraction in γ-Azido-Butyrophenones: Formation of 1,5 Ketyl Iminyl Radicals. *Org. Lett.* **2009**, *11*, 2345−2348.
(42) Sarkar, S. K.; Upul Ranaweera, R. A. A.; Merugu, R.; Abdelaziz, N. M.; Robinson, J.; Day, H. A.; Krause, J. A.; Gudmundsdottir, A. D. Comparison of the Photochemistry of Acyclic and Cyclic 4-(4-Methoxy-Phenyl)-4-Oxo-but-2-Enoate Ester Derivatives. *J. Phys. Chem. A* **2020**, *124*, 7346−7354.
(43) Sayre, H.; Milos, K.; Goldcamp, M. J.; Schroll, C. A.; Krause, J. A.; Baldwin, M. J. Mixed-Donor, α-Hydroxy Acid-Containing Chelates for Binding and Light-Triggered Release of Iron. *Inorg. Chem.* **2010**, *49*, 4433−4439.
(44) Becke, A. D. Density-Functional Thermochemistry. III. The Role of Exact Exchange. *J. Chem. Phys.* **1993**, *98*, 5648−5652.
(45) McGlynn, S. P.; Azumi, T.; Kinoshita, M. *Molecular Spectroscopy of the Triplet State*. 1969.
(46) Haag, R.; Wirz, J.; Wagner, P. J. The Photoenolization of 2-Methylacetophenone and Related Compounds. *Helv. Chim. Acta* **1977**, *60*, 2595−2607.
(47) Das, A.; Thomas, S. S.; Garofoli, A. A.; Chavez, K. A.; Krause, J. A.; Bohne, C.; Gudmundsdottir, A. D. Steric Demand and Rate-Determining Step for Photoenolization of Di-ortho-Substituted Acetophenone Derivatives. *Photochem. Photobiol.* **2019**, *95*, 154−162.
(48) Das, A.; Lao, E. A.; Gudmundsdottir, A. D. Photoenolization of o-Methylvalerophenone Ester Derivative. *Photochem. Photobiol.* **2016**, *92*, 388−398.
(49) Muthukrishnan, S.; Sankaranarayanan, J.; Pace, T. C. S.; Konosonoks, A.; DeMichiei, M. E.; Meese, M. J.; Bohne, C.; Gudmundsdottir, A. D. Effect of Alkyl Substituents on Photorelease from Butyrophenone Derivatives. *J. Org. Chem.* **2010**, *75*, 1393−1401.
(50) Konosonoks, A.; Wright, P. J.; Tsao, M.-L.; Pika, J.; Novak, K.; Mandel, S. M.; Krause Bauer, J. A.; Bohne, C.; Gudmundsdóttir, A. D. Photoenolization of 2-(2-Methyl Benzoyl) Benzoic Acid, Methyl Ester: Effect of E Photoenol Lifetime on the Photochemistry. *J. Org. Chem.* **2005**, *70*, 2763−2770.
(51) Evans, D. F. 347. Magnetic Perturbation of Singlet−Triplet Transitions. Part IV. Unsaturated Compounds. *J. Chem. Soc.* **1960**, 1735−1745.
(52) Brody, S. S. Instrument to Measure Fluorescence Lifetimes in the Millimicrosecond Region. *Rev. Sci. Instrum.* **1957**, *28*, 1021−1026.
(53) Muthukrishnan, S.; Mandel, S. M.; Hackett, J. C.; Singh, P. N. D.; Hadad, C. M.; Krause, J. A.; Gudmundsdóttir, A. D. Competition between α-Cleavage and Energy Transfer in α-Azidoacetophenones. *J. Org. Chem.* **2007**, *72*, 2757−2768.
(54) DeYonker, N. J.; Cundari, T. R.; Wilson, A. K. The Correlation Consistent Composite Approach (ccCA): An Alternative to the Gaussian-n Methods. *J. Chem. Phys.* **2006**, *124*, 114104.
(55) Patel, P.; Wilson, A. K. Domain-Based Local Pair Natural Orbital Methods within the Correlation Consistent Composite Approach. *J. Comput. Chem.* **2020**, *41*, 800−813.
(56) Grimme, S.; Antony, J.; Ehrlich, S.; Krieg, H. A Consistent and Accurate Ab Initio Parametrization of Density Functional Dispersion Correction (DFT-D) for the 94 Elements H-Pu. *J. Chem. Phys.* **2010**, *132*, 154104.


https://doi.org/10.1021/acs.jpca.3c00543
J. Phys. Chem. A 2023, 127, 2765−2778

(57) Weigend, F.; Ahlrichs, R. Balanced Basis Sets of Split Valence, Triple Zeta Valence and Quadruple Zeta Valence Quality for H to Rn: Design and Assessment of Accuracy. *PhysChemChemPhys* **2005**, *7*, 3297−3305.
(58) Grimme, S.; Ehrlich, S.; Goerigk, L. Effect of the Damping Function in Dispersion Corrected Density Functional Theory. *J. Comput. Chem.* **2011**, *32*, 1456−1465.
(59) Pansini, F. N. N.; Neto, A. C.; Varandas, A. J. C. Extrapolation of Hartree−Fock and Multiconfiguration Self-Consistent-Field Energies to the Complete Basis Set Limit. *Theor. Chem. Acc.* **2016**, *135*, 261.
(60) Hill, J. G.; Peterson, K. A.; Knizia, G.; Werner, H.-J. Extrapolating MP2 and CCSD Explicitly Correlated Correlation Energies to the Complete Basis Set Limit with First and Second Row Correlation Consistent Basis Sets. *J. Chem. Phys.* **2009**, *131*, 194105.
(61) Kendall, R. A.; Dunning, T. H., Jr.; Harrison, R. J. Electron Affinities of the First-Row Atoms Revisited. Systematic Basis Sets and Wave Functions. *J. Phys. Chem.* **1992**, *96*, 6796−6806.
(62) Weigend, F.; Köhn, A.; Hättig, C. Efficient Use of the Correlation Consistent Basis Sets in Resolution of the Identity MP2 Calculations. *J. Chem. Phys.* **2002**, *116*, 3175−3183.
(63) Ortiz-Sánchez, J. M.; Gelabert, R.; Moreno, M.; Lluch, J. M. Electronic-Structure and Quantum Dynamical Study of the Photochromism of the Aromatic Schiff Base Salicylideneaniline. *J. Chem. Phys.* **2008**, *129*, 214308.
(64) Sarkar, S. K.; Weragoda, G. K.; Ranaweera, R. A. A. U.; Gudmundsdottir, A. D. Phototautomerization on the Singlet and Triplet Surface in o-Hydroxyacetophenone Derivatives in Polar Solvents. *J. Phys. Chem. B* **2015**, *119*, 2668−2676.
(65) Yang, N. C.; Rivas, C. New Photochemical Primary Process, the Photochemical Enolization of o-Substituted Benzophenones. *J. Am. Chem. Soc.* **1961**, *83*, 2213−2213.
(66) Sankaranarayanan, J.; Muthukrishnan, S.; Gudmundsdottir, A. D., Photoremovable Protecting Groups Based on Photoenolization. In *Advances in Physical Organic Chemistry*, Richard, J. P., Ed. Academic Press: 2009; Vol. *43*, pp. 39−77.
(67) Klán, P.; Šolomek, T.; Bochet, C. G.; Blanc, A.; Givens, R.; Rubina, M.; Popik, V.; Kostikov, A.; Wirz, J. Photoremovable Protecting Groups in Chemistry and Biology: Reaction Mechanisms and Efficacy. *Chem. Rev.* **2013**, *113*, 119−191.
(68) Sliwa, M.; Mouton, N.; Ruckebusch, C.; Poisson, L.; Idrissi, A.; Aloïse, S.; Potier, L.; Dubois, J.; Poizat, O.; Buntinx, G. Investigation of Ultrafast Photoinduced Processes for Salicylidene Aniline in Solution and Gas Phase: Toward a General Photo-Dynamical Scheme. *Photochem. Photobiol. Sci.* **2010**, *9*, 661−669.




https://doi.org/10.1021/acs.jpca.3c00543
*J. Phys. Chem. A* 2023, 127, 2765−2778